Frequency Agnostic Tissue Characterization in Ultrasound Imaging using Backscattered Signal Statistics

Abhinav Gadge*
Vehant Technologies
Noida, India
abhigadge12@gmail.com

Abhishek Kumar
Department of Artificial Intelligence
IIT Kharagpur, India
abhi.kumar405@gmail.com

Debdoot Sheet
Department of Electrical Engineering
IIT Kharagpur, India
debdoot@ee.iitkgp.ac.in

***Abstract*—Ultrasound (US) imaging-based tissue characterization (TC) is a vital tool for improving diagnostic accuracy by assessing tissue properties. However, existing methods often lack generalizability across varying US acquisition frequencies. This paper introduces a frequency-agnostic TC method that estimates backscattering statistical parameters and assesses the confidence of the underlying radio frequency (RF) data distribution using two approaches: (a) variational scale estimation and (b) test signal resampling. These parameters train a random forest for TC, validated on RF data acquired at 5–10 MHz. The method achieves Dice coefficients of 0.834 ± 0.040 for hyperechoic regions and 0.751 ± 0.051 for hypoechoic regions across 400 positional acquisitions.**

***Index Terms*—Breast tumor, frequency agnostic, random forest, tissue characterization, ultrasound imaging**

I. Introduction

Ultrasound (US) imaging is a valuable diagnostic tool widely used in medicine for its real-time imaging capability and safety. However, its accuracy can be limited by subjective interpretation of echogenicity, which measures how tissue reflects or absorbs US waves.

Extensive research has focused on enhancing US imaging for better clinical diagnosis and disease assessment by understanding tissue properties [1]. Among various techniques for tissue characterization (TC), the Nakagami distribution has proven effective in modelling backscattered US echoes to characterize scatterer structures and concentrations [2]. However, the accuracy of Nakagami parameter estimation depends on the size of the estimation window; incorrect sizing can result in unreliable estimates [3]. Advanced models like the generalized Nakagami distribution have been developed to address these issues. These models provide a more refined representation of backscattered echoes and demonstrate superior performance over the standard Nakagami distribution [4]. Studies with tissue-mimicking phantoms support these advancements, showing potential for improved TC [5].

Nakagami imaging has shown promise in differentiating breast masses, particularly between benign and malignant lesions, through scatterer concentration quantification [6]. However, practical applications require careful management of factors like signal-to-noise ratio (SNR) and contrast-to-noise ratio (CNR) for high-quality imaging and effective TC [7]. Additionally, texture analysis in Nakagami imaging has emerged as a valuable method for enhancing diagnostic accuracy and reducing false positives in breast tumor characterization [8]. Beyond breast tumor characterization, Nakagami imaging has been applied to monitor thermal lesions induced by high-intensity focused ultrasound (HIFU), providing insights into tissue changes post-exposure and aiding in HIFU treatment assessment [9]. Further, advanced techniques like small-window entropy parametric imaging, quantitative US spectroscopy (QUS), and fractal feature analysis from RF echo data have been explored to overcome limitations of traditional statistical parametric imaging, enhancing US-based TC [7][10][11].

This paper presents a novel, frequency-agnostic TC approach in US imaging, using Nakagami parameters and signal confidence to characterize tissues across different

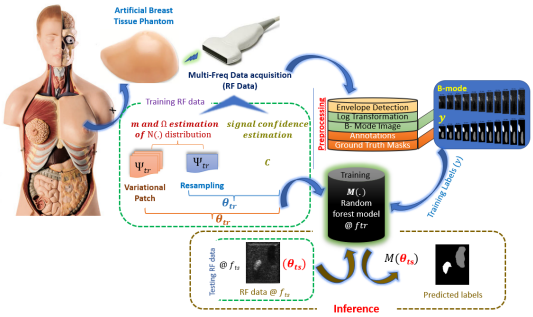

Fig. 1: The proposed method uses US imaging on an artificial breast phantom, training a random forest for TC with Nakagami parameters (m, Ω) and signal confidence (c) from RF data at a training frequency, f_{tr}. The model is applied to new RF data at a testing frequency, f_{ts}, with Nakagami parameters estimated using two methods..

*He did this work while he was student at IIT Kharagpur, West Bengal, India.

frequencies. Leveraging a wideband signal, the method effectively characterizes hypoechoic, hyperechoic, and anechoic tissues. Experimental validation on RF data from the CAE Blue Breast Phantom, demonstrates the potential of the proposed approach to improve US diagnostic accuracy and provide deeper insights into tissue properties.

II. Methods

This section is divided into four subsections, each addressing a crucial aspect of our approach. The first discusses the theoretical insights into estimating Nakagami parameters (m, Ω) and the signal confidence map (c), essential for frequency independence. The second introduces envelope detection and log compression. The third covers the estimation process using a finite sample size to maintain frequency independence. The final subsection focuses on tissue characterization (TC), where a random forest model links the estimated parameters to pixel-wise tissue segmentation and classification. An overview of the proposed method is shown in Fig. 1. Our frequency-agnostic method focuses on amplitude-based features, like the envelope (Eq.2), preserved in both RF and in-phase and quadrature-phase (IQ) formats, rather than on high-frequency oscillatory content in RF signals.

A. Parameters Estimation

1) Backscattering Statistical Physics: The echo signal received by a transducer at location x is given by:

$$S(\mathrm{x}) = \sum_{n=1}^{N} \alpha_n \cos(\omega_0 t + \Phi_n) = P\cos(\omega_0 t) - Q\sin(\omega_0 t) \quad (1)$$

where α_n and Φ_n represent the amplitude and phase of the n-th scatter, $P = \sum_{n=1}^{N} \alpha_n \cos(\Phi_n)$ is the in-phase component, $Q = \sum_{n=1}^{N} \alpha_n \sin(\Phi_n)$ is the quadrature-phase component, and N is the number of scatters. The envelope of the backscattered signal is:

$$R = \sqrt{P^2 + Q^2} \quad (2)$$

This envelope follows the Nakagami distribution [12]:

$$\mathcal{N}(r \mid m, \Omega) = \frac{2m^m r^{2m-1}}{\Gamma(m)\Omega^m} \exp\left(-m\frac{r^2}{\Omega}\right) \quad (3)$$

where r is a sample from the envelope, m is the shape parameter, and Ω is the scale parameter.

For a patch $\mathcal{P}$ of size $h \times w$ centered at r, the scale parameter Ω is calculated as:

$$\Omega = \mathbb{E}[\mathcal{P}^2] = \frac{1}{hw} \sum_{i=0}^{h-1} \sum_{j=0}^{w-1} \mathcal{P}_{i,j}^2 = (\mathbf{p} \odot \mathbf{p})\mathbf{l} \quad (4)$$

Here, $\mathbf{p}$ is the vectorized patch and $\mathbf{l}$ is a vector of ones with length hw. Thus:

The shape parameter m is:

$$m = \frac{\left(\mathbb{E}[\mathcal{P}^2]\right)^2}{\mathbb{E}[(\mathcal{P}^2 - \mathbb{E}[\mathcal{P}^2])^2]} = \frac{\Omega^2}{\mathbb{E}[\mathcal{P}^4] - \Omega^2} \quad (5)$$

For our experiments, we use a patch height h such that $\mathcal{P}_\tau$ has dimensions $(\tau + 2) \times 3$, and we set depth scale $(\tau) = 28$ to compute the parameters $\psi = \{(m_1, \Omega_1), (m_2, \Omega_2), \ldots, (m_\tau, \Omega_\tau)\}$.

2) Estimation of signal confidence: The signal confidence map (c) is calculated using the random walk algorithm, which estimates the backscattering probability for the transmitted signal [13]. We combine ψ and c to form the feature vector $(\boldsymbol{\theta})$, which has 57 dimensions (D) for a given sample r, where $\boldsymbol{\theta} = \{\psi, c\}$. An ultrasonic pulse incident on the media and the backscattered echo travelling through the heterogeneous medium is subject to the same attenuation. Therefore, the confidence of the received signal can be estimated by modelling its propagation as a random walk along an ultrasonic scanline [13]. The confidence (c) of the received signal is defined as the likelihood that a random walker, starting at any point on the scan line, will eventually reach the virtual transducer element positioned at the scan line's origin. This approach can be analytically resolved by analogy [14], as illustrated in Fig. 2. The input to the random walker is the envelope-detected raw RF signal, and the output is the confidence value for each sample, ranging from 0 to 1. We combine ψ, which has 56 dimensions, with c to obtain the $(\boldsymbol{\theta})$, which has 57 dimensions (D) for a given sample r, evaluated using Eq. (4), Eq. (5) and given by,

$$\boldsymbol{\theta} = \{\psi, c\} = \{(m_1, \Omega_1), \ldots, (m_{\tau=28}, \Omega_{\tau=28})), c\} \quad (6)$$

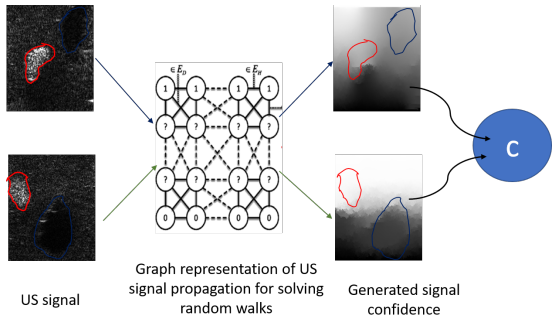

Fig. 2: Signal confidence estimation for each envelope-detected RF signal sample. The random walk algorithm calculates the probability of a walker starting at a node and reaching virtual transducer elements, identifying regions: Red (Hyperechoic) and blue (Hypoechoic).

B. Envelope Detection and Log Transformation in US Imaging

As shown in Fig 1, envelope detection in US imaging extracts the amplitude of the backscattered RF signal, with E_{max} and E_{min} as the maximum and minimum envelope values. This is achieved through rectification, low-pass filtering, and a Hilbert transform. Logarithmic transformation compresses the dynamic range of envelope data to enhance low-contrast features into B-mode images, with gray levels from 0 to 255, described by Eq. (7), Eq. (8), and Eq. (9).

$$\mathbf{B} = \alpha + \beta \log_{10}(\mathbf{E} + \gamma) \tag{7}$$

where $\mathbf{B}$ is B-mode image, $\mathbf{E}$ is the envelope data, α is a constant offset, β is a log scalar, and γ is set to 1. For each frequency, α_f and β_f are estimated as:

$$\beta_f = \frac{255}{\log_{10}\left(\frac{E_{max}}{E_{min}}\right) + 1} \tag{8}$$

$$\alpha_f = -\beta_f \log_{10}(E_{min}) \tag{9}$$

C. Approach

In US imaging, the resolution is proportional to the wavelength $\lambda = \frac{c_s}{f}$, where c_s is the speed of sound and f the frequency. According to the Nyquist theorem [15], the sampling rate must be at least twice the highest frequency to ensure accurate signal reconstruction.

For two frequencies, f_1 and f_2, the number of wavelengths in a given depth d is inversely proportional to the frequency, with the wavelength $\lambda_1 = \frac{c_s}{f_1}$ and the number of wavelengths given by:

$$N_{\lambda_1} = \frac{d}{\lambda_1} = d\frac{f_1}{c_s} \tag{10}$$

The sampling rate required for frequency f_1 is twice the number of wavelengths, given by; $N_{s_1} = 2N_{\lambda_1}$, therefore for frequency f_2, with frequency factor $F_{f_2,f_1} = \frac{f_2}{f_1}$, the required sampling rate becomes:

$$N_{s_2} = F_{f_2,f_1} N_{s_1} \tag{11}$$

Here, Eq.(10) and Eq.(11) summarize that increasing frequency leads to a shorter wavelength and a higher sampling rate. The Nakagami distribution [4] is used to model the variations in the signal due to absorption and attenuation.

1) Variation in Patch Height: US signals vary in sample count with frequency. The patch height is adjusted according to the frequency factor for accurate parameter estimation. For example, if training data is at $f_{tr} = 5$ MHz and testing is done at $f_{ts} = 8$ MHz (Fig 3):

$$F_{f_{ts},f_{tr}} = \frac{f_{ts}}{f_{tr}} = \frac{8}{5} \tag{12}$$

The patch height for test data is scaled by this factor:

$$h_{f_{ts},\tau} = F_{f_{ts},f_{tr}} h_{f_{tr},\tau} \tag{13}$$

For training data at a base frequency of 5 MHz, with depth scales $\tau = \{1, 2, \ldots, 28\}$, the patch height varies with the depth scales, which signifies the distance from the transducer to the point being imaged and is given by:

$$h_{5,\tau} = (\tau + 2) \tag{14}$$

Considering any other training frequency f_{tr}, the corresponding patch height varies as:

$$h_{f_{tr},\tau} = F_{f_{tr},5} h_{5,\tau} \tag{15}$$

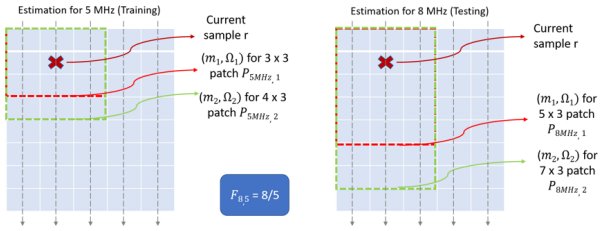

Fig. 3: Computation of Nakagami parameters with variational patch height approach for a sample r at different scales. Training data is at 5 MHz (left), where patch height is computed using Eq.(15) and testing data at 8 MHz (right), where patch height is calculated using Eq.(13)

2) Resampling the Test Data: Resampling adjusts the sampling rate by interpolation or decimation. For upsampling, zeros are inserted between samples based on the resampling ratio. A low-pass filter is used to remove high-frequency components for downsampling.

To match the number of samples between test and training data, if $f_{tr} > f_{ts}$, interpolation is applied; if $f_{tr} < f_{ts}$, decimation is used. Resampling involves:

1) Computing the Discrete Fourier Transform (DFT):

$$S[z] = \sum_{k=0}^{K-1} s[k] e^{-\frac{2\pi i z}{K}} \tag{16}$$

2) Zero-padding the DFT:

$$S_p[z] = \begin{cases} S[z] & \text{if } z < \frac{l}{2} \text{ or } z \geq K - \frac{l}{2} \\ 0 & \text{if } \frac{l}{2} \leq z < K - \frac{l}{2} \end{cases} \tag{17}$$

3) Computing the Inverse Fourier Transform (IFT):

$$s_p[k] = \sum_{z=0}^{l-1} S_p[z] e^{\frac{2\pi i z}{l} k} \tag{18}$$

The resulting signal s_p is resampled to match the training data. Parameters $\boldsymbol{\theta}$ are estimated from this resampled data, as shown in Fig. 4.

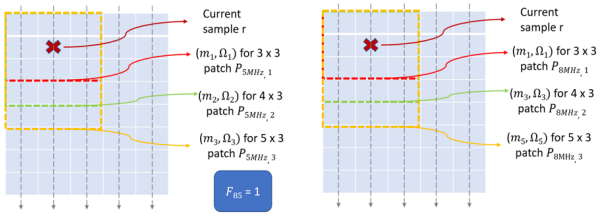

Fig. 4: Computation of Nakagami parameters with a resampling approach for a sample r at different scales for training at 5 MHz and testing at 8 MHz. The test data is resampled using Eq.(16), Eq.(17), and Eq.(18) to match the number of samples in the training data.

D. Tissue Characterization

The estimated parameters ψ and c are combined into a feature vector $\boldsymbol{\theta}$, which is used to train a random forest classifier. This classifier fits several decision trees on various dataset subsamples. The likelihood $p(r \mid y)$ of a sample r given a tissue type y can be expressed in terms of $\boldsymbol{\theta}$ as:

$$p(r; \ldots | y) \propto \{\psi, c\} \propto \boldsymbol{\theta} \tag{19}$$

Thus, the posterior probability $p(y|\boldsymbol{\theta}; r)$ is:

$$p(y|\boldsymbol{\theta}; r) = \frac{p(r; \boldsymbol{\theta}|y)}{p(r; \boldsymbol{\theta})} p(y) \tag{20}$$

where $p(y|r; \boldsymbol{\theta})$ represents the probability of tissue type y given feature parameters $\boldsymbol{\theta} = \{\psi, c\}$ as mentioned in Eq. 6. The problem is framed as a transfer learning task, where:

- $\mathcal{R}_{tr}$ is the set of training signals $\{r_{tr}\}$ at frequency f_{tr}.
- $\mathcal{R}_{ts}$ is the set of testing signals $\{r_{ts}\}$ at frequency f_{ts}.

For a training sample $r_{tr} \in \mathcal{R}_{tr}$ with feature vector $\boldsymbol{\theta}_{tr}$ and a test sample $r_{ts} \in \mathcal{R}_{ts}$ with $\boldsymbol{\theta}_{ts}$, the probability of tissue type y is given by:

$$p(y|\boldsymbol{\theta}_{ts}; r_{ts}) = \frac{p(r_{ts}; \boldsymbol{\theta}_{ts}|y)}{p(r_{ts}; \boldsymbol{\theta}_{ts})} p(y) = M(y|\boldsymbol{\theta}_{tr}, r_{tr}; \mathcal{R}_{tr}) \tag{21}$$

The random forest model $M(y|\boldsymbol{\theta}_{tr}, r_{tr}; \mathcal{R}_{tr})$ is trained on features extracted at frequency f_{tr}. This model adapts the learned parameters using features $\boldsymbol{\theta}_{tr}$ from the training data to classify test data. The source and target domains contain US signals from similar tissue types but different frequencies. The model uses these features to predict tissue type $y \in \{\text{hyperechoic, hypoechoic, isoechoic}\}$ using Eq.(20), and Eq. (21), leveraging non-linear relationships as illustrated in previous studies [16].

III. Results and Discussion

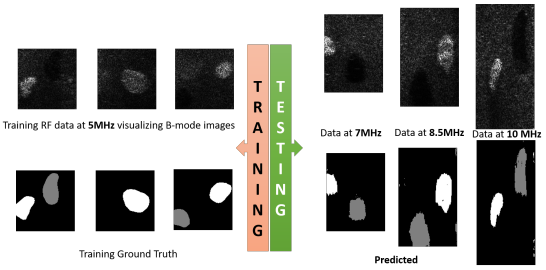

Fig. 5: Model trained with parameters $\boldsymbol{\theta}_{tr}$ from data acquired at 5 MHz, tested at 7 MHz, 8.5 MHz, and 10 MHz.

Fig. 5 illustrates the model's predictions using training data at 5 MHz and testing data at 7 MHz, 8.5 MHz, and 10 MHz. Fig. 6 shows the Dice coefficients for tissue region segmentation across these frequencies. Additionally, Fig. 7 presents semantic segmentation results, demonstrating under-segmented, over-segmented, and correctly segmented regions, highlighting the model's precision in tissue differentiation. The proposed method uses the Verasonics[1] research platform for acquiring the RF data, effectively characterizing background and tissue regions.

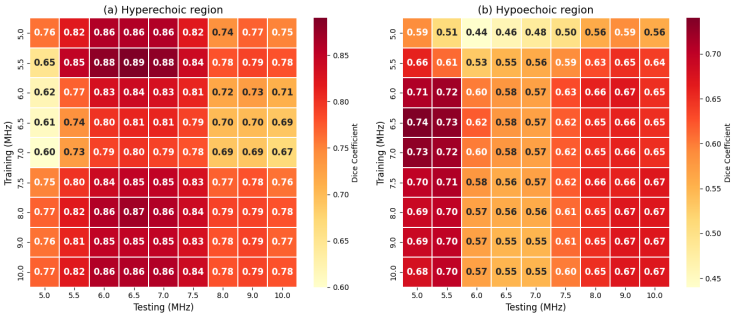

Fig. 6: Dice coefficient matrix for training and testing hypoechoic and hyperechoic tissue regions.

This work introduces a novel, frequency-agnostic approach to tissue characterization, incorporating Backscattering Statistical Physics and Signal Confidence techniques. Compared to conventional methods, it improves accuracy in identifying isoechoic, hypoechoic, and hyperechoic regions while adapting effectively to varying testing conditions. This approach surpasses existing techniques in both versatility and reliability [17] [18] [19], with future validation planned on real tumorous tissues.

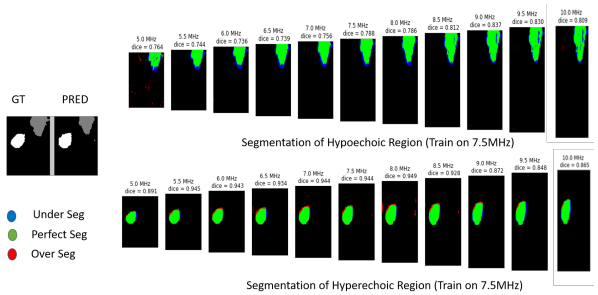

Fig. 7: Semantic segmentation of hypoechoic and hyperechoic regions, showing under, over, and perfect segmentations. Model trained on 7.5 MHz data and tested across 5 MHz to 10 MHz with 0.5 MHz intervals. Dice values for each result are shown above the images.

IV. Conclusion

In this work, we characterized tissue regions using a frequency-agnostic approach comprising two sub-methods: Backscattering Statistical Physics and Signal Confidence. This method successfully characterized the background, hypoechoic, and hyperechoic regions in tissues acquired using the Verasonics platform. In future, we plan to apply our method to actual tumorous tissues to illustrate further and validate our algorithm's results.

[1]https://verasonics.com/vantage-systems/

REFERENCES

[1] Guy Cloutier, François Destrempes, François Yu, and An Tang, "Quantitative ultrasound imaging of soft biological tissues: a primer for radiologists and medical physicists," *Insights into Imaging*, vol. 12, pp. 1–20, 2021.

[2] P.M. Shankar, "Ultrasonic tissue characterization using a generalized nakagami model," *IEEE Transactions on Ultrasonics, Ferroelectrics, and Frequency Control*, vol. 48, no. 6, pp. 1716–1720, 2001.

[3] A. Larrue and J.A. Noble, "Nakagami imaging with small windows," in *IEEE International Symposium on Biomedical Imaging: From Nano to Macro*, 2011, pp. 887–890.

[4] P Mohana Shankar, "Ultrasonic tissue characterization using a generalized nakagami model," *IEEE transactions on ultrasonics, ferroelectrics, and frequency control*, vol. 48, no. 6, pp. 1716–1720, 2001.

[5] Po-Hsiang Tsui, Chih-Kuang Yeh, Chien-Cheng Chang, and Wen-Shiang Chen, "Performance evaluation of ultrasonic nakagami image in tissue characterization," *Ultrasonic imaging*, vol. 30, no. 2, pp. 78–94, 2008.

[6] Sabiq Muhtadi, Rezwana R Razzaque, Ahmad Chowdhury, Brian S Garra, and S Kaisar Alam, "Texture quantified from ultrasound nakagami parametric images is diagnostically relevant for breast tumor characterization," *Journal of Medical Imaging*, vol. 10, no. S2, pp. S22410–S22410, 2023.

[7] Po-Hsiang Tsui, Chin-Kuo Chen, Wen-Hung Kuo, King-Jen Chang, Jui Fang, Hsiang-Yang Ma, and Dean Chou, "Small-window parametric imaging based on information entropy for ultrasound tissue characterization," *Scientific reports*, vol. 7, no. 1, pp. 41004, 2017.

[8] Ahmad Chowdhury, Rezwana R Razzaque, Sabiq Muhtadi, Ahmad Shafiullah, Ehsan Ul Islam Abir, Brian S Garra, and S Kaisar Alam, "Ultrasound classification of breast masses using a comprehensive nakagami imaging and machine learning framework," *Ultrasonics*, vol. 124, pp. 106744, 2022.

[9] Parisa Rangraz, Hamid Behnam, and Jahan Tavakkoli, "Nakagami imaging for detecting thermal lesions induced by high-intensity focused ultrasound in tissue," *Proceedings of the Institution of Mechanical Engineers, Part H: Journal of Engineering in Medicine*, vol. 228, no. 1, pp. 19–26, 2014.

[10] Laurentius O Osapoetra, Lakshmanan Sannachi, Daniel DiCenzo, Karina Quiaoit, Kashuf Fatima, and Gregory J Czarnota, "Breast lesion characterization using quantitative ultrasound (qus) and derivative texture methods," *Translational Oncology*, vol. 13, no. 10, pp. 100827, 2020.

[11] Mehdi Moradi, Parvin Mousavi, and Purang Abolmaesumi, "Tissue characterization using fractal dimension of high frequency ultrasound rf time series," in *Medical Image Computing and Computer-Assisted Intervention–MICCAI: 10th International Conference*. Springer, 2007, pp. 900–908.

[12] P Mohana Shankar, VA Dumane, John M Reid, Vladimir Genis, Flemming Forsberg, Catherine W Piccoli, and Barry B Goldberg, "Classification of ultrasonic b-mode images of breast masses using nakagami distribution," *IEEE transactions on ultrasonics, ferroelectrics, and frequency control*, vol. 48, no. 2, pp. 569–580, 2001.

[13] A Karamalis, W Wein, T Klein, and N Navab, "Ultrasound confidence maps using random walks," *Medical image analysis*, vol. 16, no. 6, pp. 1101–1112, 2012.

[14] L. Grady, "Random walks for image segmentation," *IEEE Transactions on Pattern Analysis and Machine Intelligence*, vol. 28, no. 11, pp. 1768–1783, 2006.

[15] PP Vaidyanathan, "Generalizations of the sampling theorem: Seven decades after nyquist," *IEEE Transactions on Circuits and Systems I: Fundamental Theory and Applications*, vol. 48, no. 9, pp. 1094–1109, 2001.

[16] Lidia Auret and Chris Aldrich, "Interpretation of nonlinear relationships between process variables by use of random forests," *Minerals Engineering*, vol. 35, pp. 27–42, 08 2012.

[17] E.G.T. Jaspers and P.H.N. de With, "Bandwidth reduction for video processing in consumer systems," *IEEE Transactions on Consumer Electronics*, vol. 47, no. 4, pp. 885–894, 2001.

[18] Erin A. Miller, Timothy A. White, Benjamin S. McDonald, Allen Seifert, and Michael J. Flynn, "Phase contrast x-ray imaging signatures for homeland security applications," in *IEEE Nuclear Science Symposium & Medical Imaging Conference*, 2010, pp. 896–899.

[19] E.G.T. Jaspers and P.H.N. de With, "Bandwidth reduction for video processing in consumer systems," *IEEE Transactions on Consumer Electronics*, vol. 47, no. 4, pp. 885–894, 2001.